Tunable electronic correlation effects in nanotube-light interactions

AUTHOR(S):

Miyauchi, Yuhei; Zhang, Zhengyi; Takekoshi, Mitsuhide; Tomio, Yuh; Suzuura, Hidekatsu; Perebeinos, Vasili; Deshpande, Vikram V.; ... Kim, Philip; Hone, James; Heinz, Tony F.

CITATION:

Miyauchi, Yuhei ...[et al]. Tunable electronic correlation effects in nanotube-light interactions. Physical Review B 2015, 92(20): 205407.

ISSUE DATE:

2015-11-04

URL:

http://hdl.handle.net/2433/207610

PHYSICAL REVIEW B **92**, 205407 (2015)

Tunable electronic correlation effects in nanotube-light interactions

Yuhei Miyauchi,[1,2,3,*] Zhengyi Zhang,[4,5] Mitsuhide Takekoshi,[6] Yuh Tomio,[7] Hidekatsu Suzuura,[7] Vasili Perebeinos,[8,9] Vikram V. Deshpande,[10,11] Chenguang Lu,[12,13] Stéphane Berciaud,[14] Philip Kim,[11] James Hone,[4] and Tony F. Heinz[3,†]

[1]*Institute of Advanced Energy, Kyoto University, Gokasho, Uji 611-0011, Japan*
[2]*Graduate School of Science, Nagoya University, Chikusa, Nagoya 464-8602, Japan*
[3]*Departments of Physics and Electrical Engineering, Columbia University, New York, New York 10027, USA*
[4]*Department of Mechanical Engineering, Columbia University, New York, New York 10027, USA*
[5]*SanDisk, 951 SanDisk Drive, Milpitas, California 95035, USA*
[6]*Department of Electrical Engineering, Columbia University, New York, New York 10027, USA*
[7]*Division of Applied Physics, Graduate School of Engineering, Hokkaido University, Sapporo 060-8628, Japan*
[8]*IBM Research Division, T. J. Watson Research Center, Yorktown Heights, New York 10598, USA*
[9]*Skolkovo Institute of Science and Technology, 3 Nobel Street, Skolkovo 143025, Russian Federation*
[10]*Department of Physics & Astronomy, University of Utah, Salt Lake City, Utah 84112, USA*
[11]*Department of Physics, Columbia University, New York, New York 10027, USA*
[12]*Department of Applied Physics and Applied Mathematics, Columbia University, New York, New York 10027, USA*
[13]*National Center for Nanoscience and Technology, Beijing 100080, China*
[14]*Institut de Physique et Chimie des Matériaux de Strasbourg and NIE, UMR 7504, Université de Strasbourg and CNRS, 23 rue du Loess, Boîte Postale 43, 67034 Strasbourg Cedex 2, France*

(Received 2 September 2013; revised manuscript received 16 August 2015; published 4 November 2015)

Electronic many-body correlation effects in one-dimensional (1D) systems such as carbon nanotubes have been predicted to strongly modify the nature of photoexcited states. Here we directly probe this effect using broadband elastic light scattering from individual suspended carbon nanotubes under electrostatic gating conditions. We observe significant shifts in optical transition energies, as well as line broadening, as the carrier density is increased. The results demonstrate the role of screening of many-body electronic interactions on the different length scales, a feature inherent to quasi-1D systems. Our findings further demonstrate the possibility of electrical tuning of optical transitions and provide a basis for understanding of various optical phenomena in carbon nanotubes and other quasi-1D systems in the presence of charge carrier doping.

DOI: 10.1103/PhysRevB.92.205407 PACS number(s): 78.67.Ch, 71.35.−y, 73.22.−f, 78.35.+c

I. INTRODUCTION

Quantum many-body correlation effects in photon-matter interactions have long been a subject of central importance in condensed-matter physics. Understanding of these effects in quasi-one-dimensional (1D) systems, where their influence is generally far more pronounced than in bulk materials [1,2], has been a focus of particular attention. In this context, single-walled carbon nanotubes (hereafter referred to as nanotubes) provide the ultimate limit for quasi-1D quantum wires. They have diameters on the order of 1 nm and shells of single-atom thickness. Photoexcited electrons and holes in semiconducting nanotubes form stable two-particle excitonic bound states through their mutual Coulomb attraction, with binding energies of hundreds of meV [2–9]. Excitons in nanotubes are therefore highly stable at room temperature, unlike the case for conventional semiconductor quantum wires. Additionally, one can tune the carrier density and Fermi energy in nanotubes widely by means of electrostatic gating [10–14]. Nanotubes thus offer an ideal platform for the fundamental studies of the many-body interactions and their impact on the optical spectra of photoexcited quasi-1D systems [2–9,11–60]. Knowledge of the underlying optical response of nanotubes under carrier doping is also of great importance for the development of electrically tunable optoelectronic devices [11–13,56,59] that operate at room temperature and on the nanometer length scale. For a complete understanding of the impact of many-body electronic correlation effects on the optical response, it is highly desirable to observe broadband optical response of clean and isolated 1D nanostructures over a wide range of free-carrier densities.

Here we demonstrate the direct characterization of the optical transitions as a function of carrier density using a spectroscopic technique capable of accessing individual nanotubes. The approach provides optimal conditions for the identification of many-body effects on optical transitions and for detailed examination of the underlying electron-electron, electron-hole, exciton-electron (hole), and exciton-photon interactions. Our measurements rely on broadband elastic (Rayleigh) light scattering spectroscopy [22,31] from individual, suspended carbon nanotubes [Fig. 1(a)]. The experimental configuration allows for measurement of scattering spectra under conditions of variable electrostatic gating, which provides precise control of the injected charge density in the lowest-energy bands [Fig. 1(b)]. These investigations complement studies of gate-dependent Raman [13,14,27,28,41] and photoluminescence [13,37] spectroscopy of air-suspended nanotubes, gate-dependent Rayleigh scattering spectroscopy of individual nanotubes on substrates [52], and chemically-carrier-doped nanotubes [38,44,47–49,51,53,57,61,62] showing spectral features attributed to formation of charged excitons (trions) [38].

*miyauchi@iae.kyoto-u.ac.jp
†tony.heinz@columbia.edu

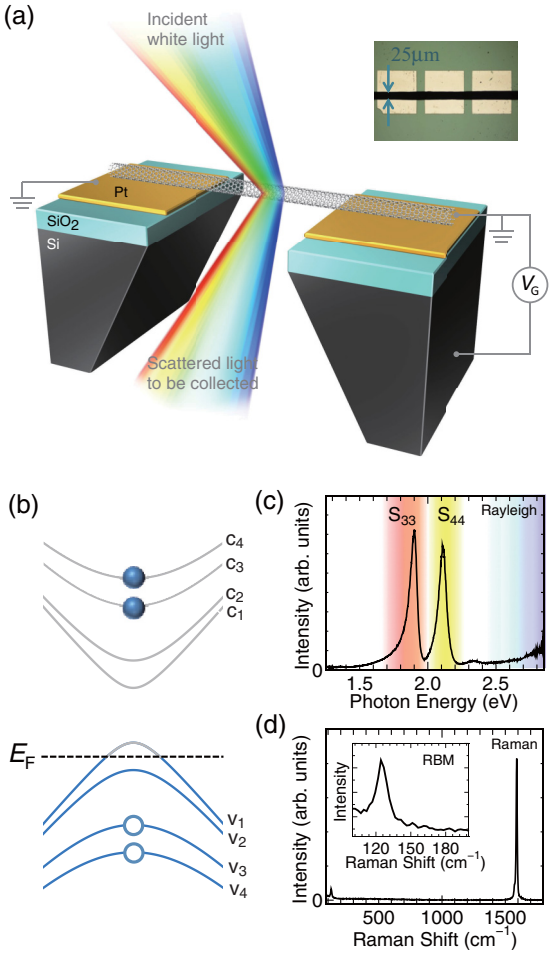

FIG. 1. (Color online) (a) Schematic of our individual nanotube device. The inset shows a microscope image of a substrate with the slit and electrodes used in this study. (b) Schematic diagram of the band structure of a semiconducting nanotube under electrostatic gating conditions (hole doping). (c) Elastic (Rayleigh) and (d) inelastic (Raman) light scattering spectra of a single undoped nanotube. The inset shows the spectrum around the radial breathing mode (RBM). We present all the Rayleigh spectra corrected for the ω^3 scattering efficiency factor to reflect directly the optical susceptibility.

In our investigations we observe peak shifts and broadening of exciton resonances with increasing carrier density in semiconducting nanotubes. The measured redshift of the exciton transition energies with doping indicates a reduction of strength of the Coulomb interactions, leading to a decrease in the quasiparticle band gap, partially offset by a decrease in the exciton binding energy. The magnitude of the spectral shifts with doping can be understood within the context of a length-scale-dependent dielectric screening inherent to quasi-1D systems. The width of the excitonic peak is found to increase nearly linearly with injected carrier density. This behavior is well reproduced by calculations of intervalley scattering processes involving the injected charges. Our findings provide fundamental information on the optical transitions and the role of many-body interactions in defining their characteristics in carrier-doped carbon nanotubes. The results will serve as a basis for the interpretation of various optical phenomena sensitive to the optical resonances under the doped conditions. The demonstrated tunability of exciton resonance in these systems also provides the basis for the development of alternative optoelectronics devices, such as gate-tunable photon detectors, modulators, and metamaterials.

II. EXPERIMENTAL AND THEORETICAL METHODS

A. Sample preparation and device fabrication

We examined individual single-walled carbon nanotubes prepared by ambient chemical vapor deposition methods using a modified fast-heating process [63]. The nanotubes were grown directly over open slits of 20–30 μm width cut in SiO_2/Si substrates. The electrical contact to the nanotubes needed for gating experiments was obtained using electrodes (1 nm of tungsten and 15 nm of platinum) fabricated on both sides of the slit. The chiral indices of each nanotube spanning the slit were assigned by simultaneous Rayleigh and Raman spectroscopy [22,64]. For a nanotube employed in the measurements, we observed two distinct peaks at 1.9 and 2.1 eV in the Rayleigh scattering spectrum [Fig. 1(c)]. The features correspond, respectively, to the third and fourth subband exciton resonances (S_{33} and S_{44}). In the Raman spectrum, G-mode (at 1592 cm^{-1}) and radial breathing mode (at 125 cm^{-1}) features were observed as shown in Fig. 1(d). On the basis of these observations, the nanotube is assigned to a near-zigzag semiconducting nanotube of 2.0–2.1 nm in diameter, belonging to the family with chiral indices (n,m) satisfying $(n-m) \bmod 3 = 2$. The possible assignment of the nanotube structure is a zigzag (26, 0), or possibly neighboring near-zigzag species such as (25, 2) [22,64]. The narrow G-mode feature at 1592 cm^{-1} in the Raman spectrum indicating a dominant contribution of zone center longitudinal optical photon is also consistent with the assignment to near-zigzag semiconducting species [64]. Unwanted nanotubes were removed by intense laser irradiation to yield a clean experimental geometry for the gating measurements.

B. Optical spectroscopy under electrostatic gating conditions

Broadband light generated by a supercontinuum source (with integrated power of about 0.4 mW over the wavelength range of ~450–1100 nm, for Rayleigh spectroscopy) or monochromatic light from a laser (with power of 0.37 mW, for Raman spectroscopy) was focused at the center of an individual suspended nanotube with spot size of 2–3 μm and polarization along the nanotube axis. The scattered light was collected by a spectrometer through a confocal arrangement [22]. The gate bias for electrostatic doping was applied to the silicon substrate. The gate electric field from the sidewalls of the slit served to tune the Fermi energy and carrier density in the nanotube [Fig. 1(b)]. The gate capacitance of the device $C_G = 0.018e/V\,nm$ was determined using the variation of Raman scattering spectra from a chiral metallic nanotube under gating conditions (see Appendix A for details). We confirmed experimentally that the inhomogeneity of the gating efficiency within a region of ±7.5 μm from the center of a nanotube was negligible by comparing the Rayleigh spectra taken at the different positions along the nanotube under the gating conditions. All measurements were conducted under a nitrogen

gas environment to prevent any possible modification from ambient air, for example, through H_2O or O_2 adsorption.

C. Theoretical treatment

The S_{33} and S_{44} exciton energies dependent on carrier density are predicted within a $\boldsymbol{k}\cdot\boldsymbol{p}$ scheme by solving the Bethe-Salpeter (BS) equation. In the calculation, exciton states are determined by a circumferential length $L_c(=\pi d)$ of the nanotube, a characteristic kinetic energy $2\pi\gamma/L_c$ [$\gamma=(\sqrt{3}/2)a\gamma_0$ with nearest-neighbor hopping integral $\gamma_0=2.7\,\mathrm{eV}$ and a lattice constant $a=2.46\,\text{Å}$ of graphene], and a characteristic Coulomb energy $e^2/\kappa L_c$, where κ is an effective dielectric constant accounting for the effects of polarization of surrounding materials and electrons far from the Fermi level. The dimensionless Coulomb parameter $v=(e^2/\kappa)/(2\pi\gamma)$ represents the Coulomb interaction $e^2/\kappa L_c$ scaled by the characteristic kinetic energy. In the calculations we use, $v=0.16$, corresponding to $\kappa=2.5$. In our $\boldsymbol{k}\cdot\boldsymbol{p}$ treatment, we consider intravalley Coulomb interactions near the K (K') valley of the graphene Brillouin zone. We calculate the screened Coulomb interaction that depends on the carrier density and the relevant length scale of the interactions within the static random-phase approximation.

To calculate the decay rates and line broadening of the excitonic transitions we consider the process in which a photoexcited electron-hole pair in the third (or fourth) subband scatters with injected electrons or holes in the first subband. We evaluate the corresponding rates within the second-order perturbation theory, and treat the intervalley scattering pathways with the same Coulomb parameters as were used for the calculation of the peak shifts. As expected, a peak shift also arises from these intervalley scattering processes. The calculated shift at $\rho=0.42\,e/\mathrm{nm}$ ($\sim$2.6 meV) is, however, far smaller than the experimental shift ($\sim$60 meV) in Fig. 3. Hence, we can safely neglect the effect of the intervalley processes in describing doping-induced shifts of the excitonic transition energies. All the calculations were conducted on a (26, 0) semiconducting nanotube for comparison with the experimental results. More detailed descriptions of the calculation of the energy shift and broadening are presented in Appendixes B and C.

III. RESULTS AND DISCUSSION

A. Rayleigh scattering spectra under electrostatic gating conditions

Under the application of a gate bias voltage V_G to inject charge into the suspended semiconducting nanotube, we observed clear shifts in the peak positions of the S_{33} and S_{44} transitions, as well as broadening of the features with increasing $|V_G|$ (Fig. 2). The spectra are analyzed by a fitting procedure using an excitonic description of the nanotube optical response [31]. For Rayleigh scattering of a one-dimensional system, the measured scattering cross section $\sigma(\omega)$ varies with optical frequency ω as $\omega^3|\chi(\omega)|^2$, where $\chi(\omega)$ is the optical susceptibility of the nanotube. We model the nanotube excitonic response by a Lorentzian line shape of the form $\chi=\chi_b+f[(\omega_0-\omega)-i\Gamma/2]^{-1}$. Here χ_b is the (frequency-independent) background susceptibility arising

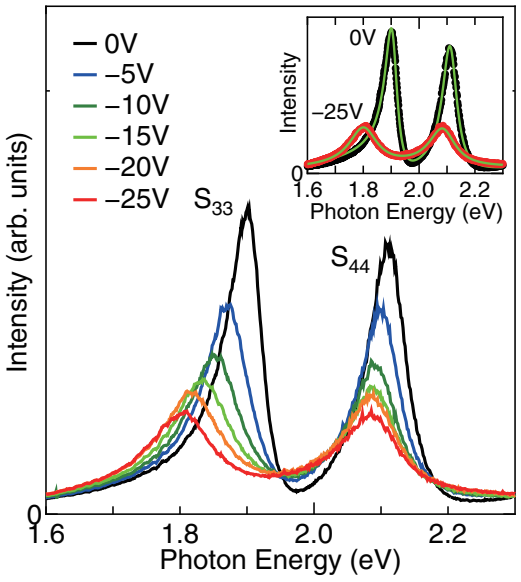

FIG. 2. (Color online) Rayleigh scattering spectra for the observed semiconducting nanotube for gating voltages from $V_G=0$ to -25 V. Similar spectral changes were observed for positive gating voltages (Supplemental Material [65]). The inset shows Rayleigh scattering spectra of the semiconducting nanotube at $V_G=0$ V (black solid circles) and $V_G=-25$ V (red solid circles). The solid green curves are fits based on an excitonic model of the optical susceptibility described in the text.

from the nonresonant transitions, f is a parameter proportional to the exciton oscillator strength, ω_0 is the resonance frequency, and Γ is the linewidth of the transition. This fitting procedure has been successfully applied for higher-order Rayleigh scattering peaks of metallic and semiconducting nanotubes [31].

This model generates excellent fits to the experimental scattering spectra (Fig. 2). For clarity, we discuss the results for negative gate bias voltages V_G, corresponding to hole doping; the results for electron doping are similar (see Supplemental Material [65]). Note that the decrease of the peak height for the large $|V_G|$ primarily originates from line broadening, and there is no meaningful reduction in the oscillator strength parameter f, as confirmed by the fit. We thus stress that the S_{33} and S_{44} bands are not directly filled by the injected electrons or holes within the observed range of $|V_G|$. These carriers reside only within the lowest-energy bands [Fig. 1(b)]. Thus, simple Pauli blocking effects influence only the S_{11} transition. By observing the higher-order S_{33} and S_{44} transitions, we directly probe the modification of the *many-body interactions* induced by the free-carrier density.

B. Exciton energy shift

The experimentally determined shift in the exciton transition energies of the near-zigzag semiconducting nanotube as a function of the injected carrier density ρ is presented in Fig. 3(a). In order to focus on modifications of the electronic many-body interactions under the gating conditions, we plot the average value $\Delta E_{av}\equiv(\Delta E_{33}+\Delta E_{44})/2$ of the shifts of S_{33} and S_{44} peaks. This procedure eliminates the

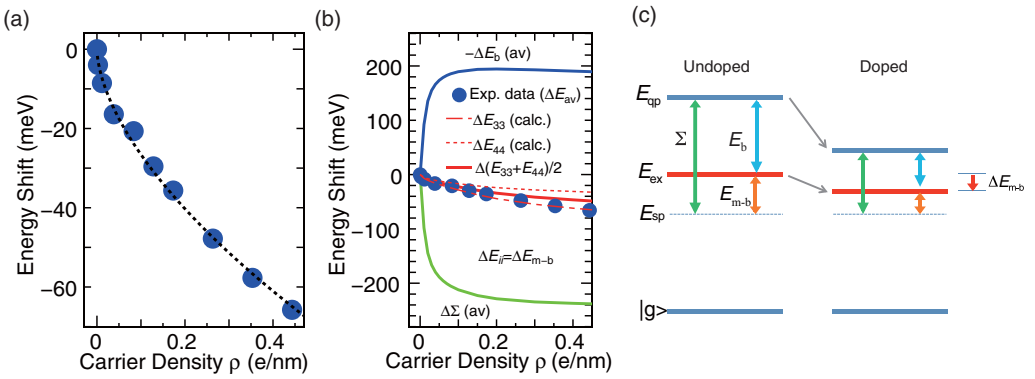

FIG. 3. (Color online) (a) Dependence of the exciton resonance energy shifts of the semiconducting nanotube on the carrier (hole) density. The dotted curve indicates a power-law function. (b) Calculated S_{33} and S_{44} shifts of the exciton transition energies ΔE_{33} and ΔE_{44} (red dot-dashed and dotted curves) and their average (red solid curve) for a (26, 0) nanotube as a function of carrier density ρ. The calculated changes in E_b and $\Sigma(\Delta E_b$ and $\Delta\Sigma)$ (blue and green curves, averaged for S_{33} and S_{44} excitons), and the experimental data ΔE_{av} shown in (a) (blue circles) are plotted together for comparison. (c) Schematic diagram of the physical mechanisms for the redshift in the transition energy with doping.

effect from electrostatically induced strain (see Supplemental Material [65]), which causes the two peaks to shift in opposite directions, but does not change their average position [66]. Here we denote the strain-induced peak shift of S_{ii} transition as $\Delta E_{ii}^{\rm st}$ and the purely electronic contribution (the peak shift from modification of many-body interactions) as $\Delta E_{ii}^{\rm el}$. The total peak shift, $\Delta E_{ii} = \Delta E_{ii}^{\rm st} + \Delta E_{ii}^{\rm el}$, is the sum of the strain and electronic contributions. According to an earlier study [66], the strain-induced peak shift for the S_{33} and S_{44} satisfies $\Delta E_{33}^{\rm st} = -\Delta E_{44}^{\rm st}$ to a high degree of accuracy. Thus, the average peak shift of the two transitions, $\Delta E_{\rm av} = (\Delta E_{33}^{\rm el} + \Delta E_{44}^{\rm el})/2$, can be considered as reflecting only the influence of the *electronic* contributions. We found that the observed redshift of the averaged exciton energy of the semiconducting nanotube with charge density ρ is reproduced using a power-law function of the form $\Delta E_{\rm av} = A\rho^{\alpha}$ [dotted line in Fig. 3(a)], with an exponent of $\alpha = 0.6$ and a prefactor of $A = 106\,{\rm meV\,nm}^{0.6}$.

For the observed peak shift, we first consider the possible influence of the direct contribution of the applied electric field on the excitonic transition energies, i.e., the potential role of the dc Stark effect in the nanotube on our experimental measurement. For geometries in which no charging of the nanotube is expected, prior theoretical studies [67] predicted that a Stark shift on the order of 200 meV for a transverse electric field of 6.7 MV/cm for a zigzag nanotube of a similar diameter to our semiconducting nanotube. In our case, we estimate an effective transverse applied field on the order of 0.01 MV/cm, implying a Stark effect of at most 0.3 meV [67], far less than our observed spectral shifts. In addition, prior experimental investigations reported the absence of any detectable spectral shifts for transverse electric fields up to 0.2 MV/cm [68], and a shift of 0.35 meV for a transverse field of 1.6 MV/cm [69]. On this basis, we ignore the role of the dc Stark effect in our measurements.

We also evaluate the possible effect of trion formation in the Rayleigh scattering spectra. In carbon nanotubes, the trion binding energy (the energy separation between the exciton and trion peaks) has been reported to be much larger (more than 100–200 meV [38] for S_{11} excitons) than that of conventional semiconductors because of strong electron-hole exchange interactions in nanotubes. For the higher-order excitons S_{33} and S_{44} with larger effective masses, we expect comparable or even larger energy separation between the exciton and trion peaks. Hence, the energy separation of the exciton and trion peaks is expected to be much larger than the energy range of the observed shift and broadening of the exciton peaks. Moreover, it has been reported that the optical absorption feature from the creation of trions is much smaller (less than 1/10) than that of the exciton absorption feature even under conditions of relatively heavy doping using chemical treatments [38], presumably because of the small oscillator strength of trions [57]. In the case of Rayleigh scattering spectra, the peak intensity from the creation of trions (if present) is expected to be still smaller because Rayleigh scattering cross section is proportional to the square of the optical susceptibility. On this basis, we can exclude the effect of trion formation on the observed spectral changes.

The measured change of $\Delta E_{\rm av}$ is thus attributable simply to the consequence of the modification of the many-body interactions induced by the free-carrier density in the nanotube. In order to explore the origin of the observed peak shifts, we conducted a theoretical study of excitons under finite carrier density within the $\boldsymbol{k}\cdot\boldsymbol{p}$ approximation [2,42]. The S_{33} and S_{44} exciton energies dependent on carrier density are predicted by solving the Bethe-Salpeter (BS) equation (see Sec. II and Appendix B). Figure 3(b) displays the calculated shift for the S_{33} energy, ΔE_{33} (red dot-dashed curve), for the S_{44} exciton energy, ΔE_{44} (red dotted curve), and for their average (red solid curve) as a function of injected carrier (hole) density. The experimental data $\Delta E_{\rm av}$ are plotted together for comparison (blue circles). The trend of the experimental energy shift is well reproduced for typical Coulomb parameters (see Sec. II and Appendix B).

The calculation provides a clear perspective on the physical origin of the shift in exciton energy induced by free carriers. As shown in Fig. 3(c), the exciton transition energy $E_{\rm ex}$ is determined by

$$E_{\rm ex} = E_{\rm sp} + \Sigma - E_{\rm b}, \tag{1}$$

where E_{sp} is a single-particle gap between the relevant subbands, Σ is the self-energy correction for the quasiparticle band gap from electron exchange correlations, and E_b is the exciton binding energy from the attractive electron-hole interactions. (Here we consider Σ and E_b to be positive quantities.) Therefore, the net many-body correction energy E_{m-b} to the single-particle gap is $E_{m-b} = \Sigma - E_b$, and the exciton energy *shift* due to modified many-body interactions originates from $\Delta E_{m-b} = \Delta(\Sigma - E_b)$, as shown in Fig. 3(c).

The calculated changes in E_b and Σ(ΔE_b and $\Delta\Sigma$, averaged for S_{33} and S_{44}) are plotted in Fig. 3(b) to show separately the contributions of each component to the net exciton energy shift ΔE_{m-b}. We find that ΔE_b and $\Delta\Sigma$ cancel one another to a significant degree, but that $|\Delta\Sigma|$ is always larger than $|\Delta E_b|$. Thus a redshift of the exciton energy E_{ex} is always predicted ($\Delta E_{m-b} < 0$), in accordance with experiment. The key to understanding the mechanism of the net redshift lies in the dependence of the Coulomb interaction on the length scale [6]. The value of Σ in Eq. (1) consists of the contributions both from long-range 1D Coulomb interactions Σ_l (occurring on a length scale greater than the nanotube circumference) and from two-dimensional (2D)-like short-range interactions Σ_s (occurring on a length scale less than the circumference). Given the spatial extent of the exciton [30], the exciton binding energy E_b, on the other hand, is dominated by long-range 1D Coulomb interactions [6,43]. The changes in Σ_l and E_b relevant to the 1D Coulomb interactions are large, but cancel one another to a high degree of accuracy, whether in the neutral or doped system. Therefore, the shift in the exciton energy ΔE_{m-b} is almost completely dominated by the change in Σ_s, namely, $\Delta E_{m-b} \approx \Delta\Sigma_s$. We note that our calculations have been carried out in the limit of a static screen. Since the dynamical effects have been predicted to weaken screening of 1D interactions [36], this may lead to an underestimate of values E_b and Σ. The discussion above is, however, robust as long as the cancellation of the long-range 1D interactions is maintained.

Let us therefore consider how Σ_s is reduced with doping using our experimental observations. The exciton transition energies in our near-zigzag semiconducting nanotube show a redshift of about 60 meV or 3% of the transition energy at a charge density of $\rho = 0.4\ e$/nm. Our calculation of the excitons in a (26, 0) nanotube suggests that $E_{m-b}(\approx \Sigma_s)$ accounts for about 20% of the net transition energy in the undoped nanotube. Thus, the 3% redshift of the exciton energy corresponds to ~15% decrease in Σ_s, i.e., the short-range interaction strength is reduced to 85% of its intrinsic strength for $\rho = 0.4\ e$/nm. This tunability of the short-range interaction strength for a wide range of free-carrier density, together with the nearly perfect cancellation of Σ_l and E_b by 1D long-range interactions, makes fine control of the higher subband exciton resonance energy possible without relying on the Pauli-blocking effect in carbon nanotubes.

C. Linewidth broadening

We now consider another important experimental observation, namely, the change in the linewidth of the excitonic transitions with doping. Figure 4(a) shows the carrier density dependence of the linewidth of the S_{33} and S_{44} transitions

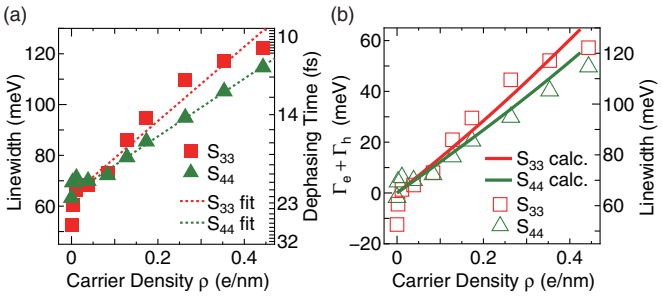

FIG. 4. (Color online) (a) Dependence of the S_{33} and S_{44} exciton resonance linewidths of the semiconducting nanotube on carrier density. The dotted lines are fits of the function $\Gamma_{ii}(\rho) = \Gamma_{ii0} + \beta_{ii}\rho$ to the linewidths for the S_{ii} exciton. The right axis indicates the dephasing time of excitons corresponding to the linewidth. (b) Calculated decay rates (red and green solid lines for S_{33} and S_{44}, respectively) of a photoexcited electron-hole pair in a (26, 0) nanotube due to the free-carrier doping. The calculated data are plotted together with the experimental data (opaque symbols) shown in (a) with 65-meV offset between the left (for calculated results) and right (for experimental data) vertical axes to account for decay channels of the undoped nanotube.

in the near-zigzag semiconducting nanotube. We find that the linewidths increase significantly with carrier density ρ. A similar effect for the higher-order transitions has been observed under strong photoexcitation regime (for S_{22}) [21] and in individual semiconducting nanotubes on substrates using an optical microscopy technique (for S_{44} and S_{55}) [52]. The linewidth of an excitonic transition reflects the rate of dephasing of the exciton coherence, and the inferred exciton dephasing times with doping are shown on the right axis of Fig. 4(a). The observed linewidth change exhibits a nearly linear increase with increasing ρ, except for the sharp increase of about 10 meV at low ρ. For densities $\rho > 0.05\ e$/nm, the experimental linewidth $\Gamma(\rho)$ can be fit with a linear function of carrier density as $\Gamma_{ii}(\rho) = \Gamma_{ii0} + \beta_{ii}\rho$, where Γ_{ii0} and β_{ii} are constants. The coefficients $\beta_{33} = 145$ meV nm and $\beta_{44} = 114$ meV nm characterize the additional contribution of doping to the dephasing of the S_{33} and S_{44} excitons.

Our theoretical treatment for the peak shift within the treatment of the BS equation also predicts the exciton linewidth as the imaginary part of the complex exciton energy. We found, however, that the additional linewidth is nearly constant for finite carrier densities of $\rho > 0.05\ e$/nm, and the linear increase of the linewidth is not reproduced. To address this discrepancy with theory, we explored possible contributions to the linewidth from the *intervalley* (K-K') interactions that were omitted within the treatment of the $\boldsymbol{k}\cdot\boldsymbol{p}$ approximation (see Sec. II and Appendix C). We consider the process in which a photoexcited electron-hole pair in the third (or fourth) subband scatters with injected electrons or holes in the first subband. The corresponding rates are evaluated within the second-order perturbation theory, treating the intervalley scattering pathways with the same Coulomb parameters as were used for the calculation of the peak shifts.

Figure 4(b) shows the calculated linewidth broadening (the sum of the decay rate of the photoexcited electron and hole $\Gamma_e + \Gamma_h$) as a function of carrier density ρ, plotted together

with the same experimental data shown in Fig. 4(a). In good agreement with experiment, we predict nearly linear increases of the linewidth of S_{33} and S_{44} transitions. The calculation also shows that the number of decay channels for photoexcited holes in the S_{44} band is smaller than that for S_{33}. This explains the counterintuitive experimental result of a slightly smaller doping-induced broadening of S_{44} width than that of S_{33}. We therefore attribute the nearly linear broadening of the linewidth with doping to intervalley scattering processes involving the injected charges.

D. Practical implications of the results

Finally, we comment briefly on some practical implications of this study. The observed tunability of the exciton resonance frequency by a full linewidth for carrier levels on the order of only 0.5 e/nm could be useful for applications such as nanosized, tunable photon detectors or modulators. Furthermore, such tunability of the optical responses may offer the possibility of constructing tunable metamaterials by integration of individual nanotubes in other structures. Our findings are also important for the interpretation of various experimental results related to the optical resonance of isolated nanotubes. In particular, our results imply that one needs to exercise considerable care in making chirality assignment of nanotubes on substrates, where unintentional doping effects may lead to a significant shift in the measured transition energies. More broadly, the strong many-body effects in these materials imply that their optical response will be significantly modified by carrier density, even in the absence of Pauli blocking effects.

IV. CONCLUSIONS

We have demonstrated that the higher-order excitonic transitions in individual suspended semiconducting carbon nanotubes exhibit significant redshifts and broadening with increasing carrier doping. These features do not arise from simple Pauli blocking, since no charge is injected into the relevant bands, but rather reflect the role of many-body electronic interactions. Our theoretical investigations show that the decrease in many-body contributions to the excited-state energy is dominated by intravalley interactions with a quasi-2D character. The nearly linear peak broadening with increased carrier density, on the other hand, has a different physical origin: It can be explained on the basis of intervalley scattering processes involving the injected carriers. These results provide a rigorous basis for the interpretation of changes in the optical response induced by carrier doping in carbon nanotubes and other quasi-1D systems; the results also suggest possibilities for gate-tunable optoelectronic devices.

ACKNOWLEDGMENTS

This research was supported by Grant-in-Aid for Scientific Research Grants No. 08J03712 and No. 24681031 from Japan Society for the Promotion of Science (JSPS) and by Precursory Research for Embryonic Science and Technology (PRESTO) Grant No. 3538 from Japan Science and Technology Agency (JST) for Y.M. The spectroscopic studies were supported by the U.S. National Science Foundations (NSF) through Grant No. DMR-1106225; device fabrication was supported by the U.S. NSF through Grant No. DMR-1006533, by the U.S. Department of Energy, Office of Basic Energy Sciences through Grant No. DE-SC0001085 for the Columbia Energy Frontier Research Center, and by the Honda Research Institute. The authors would like to thank P. Avouris and M. Freitag for fruitful discussions.

APPENDIX A: EVALUATION OF THE GATE CAPACITANCE

The gate capacitance of our nanotube devices determines the relationship between the applied voltage and the physically important induced charge density. We evaluated this quantity using Raman scattering spectroscopy of a chiral *metallic* nanotube suspended over the same slit where the near-zigzag semiconducting nanotube employed in the measurements described in the main text was located. For a chiral metallic nanotube, the linewidth of the G^- Raman mode is known to change systematically as a function of the charge density because of the dependence of the phonon lifetime [28,70] on the position of the Fermi energy E_F. Thus, this nanotube provides an excellent sample for calibration of induced charge density.

Figure 5 displays the change in the G-mode Raman spectra for the different electrostatic gating conditions of the metallic nanotube. The broad background in the spectrum at 0 V arises from electronic Raman scattering [41] and has been subtracted out for the linewidth analysis. The inset in Fig. 5 displays the measured gate dependence of the linewidth of the G mode (red circles). We fit these data considering the gate-variable electron-phonon coupling [28,70], which can be approximated as

$$\Gamma(E_F) = \Gamma_0 + \Gamma_{e-ph}[f(T, E_F, -E_{ph}/2) - f(T, E_F, E_{ph}/2)]. \quad \text{(A1)}$$

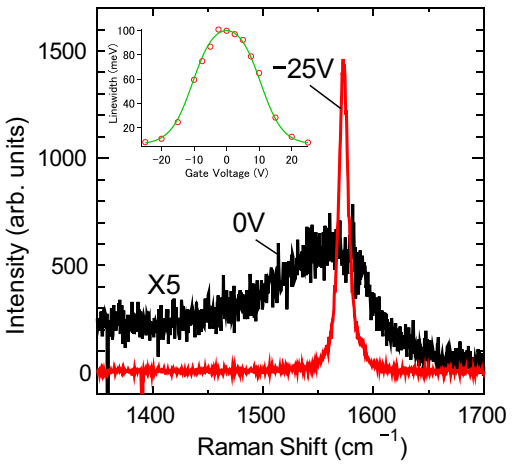

FIG. 5. (Color online) Raman G-mode spectra for gate voltages of $V_G = 0$ (black curve) and -25 V (red curve) taken from an individual chiral metallic nanotube suspended over the same slit where the near-zigzag semiconducting nanotube employed in the measurements described in the main text was located. The inset displays the measured width of this mode (red circles) as a function of the gate voltage V_G. The green curve is a fit to Eq. (A1) for the variation with charge density.

Here Γ_0 and $\Gamma_{e-\mathrm{ph}}$ are constants, E_{ph} is the energy of the G^- phonon, and $f(T, E_{\mathrm{F}}, E)$ is the Fermi distribution function at temperature T, where we have neglected the effect of the finite temperature on the chemical potential μ and have set $\mu = E_{\mathrm{F}}$. In the fit, we assume that the Fermi energy E_{F} in the metallic nanotube is directly proportional to the gate voltage V_{G}. In filling the linearly dispersing metallic band, this assumption is equivalent to that of a direct proportionality between V_{G} and the induced charge density in the nanotube, i.e., as expected for a constant gate capacitance.

From the fit above and the relation $\rho = 4E_{\mathrm{F}}/\pi\hbar v_{\mathrm{F}}$ for charge density in a metallic band with Fermi velocity $v_{\mathrm{F}} \approx 10^6$ m/s, we obtain an effective gate capacitance of $C_{\mathrm{G}} = 0.018e/\mathrm{V\,nm}$. Given the range of applied voltages and the shift in the Fermi level, we are justified in neglecting the effect of quantum capacitance of the nanotube [71] and considering C_{G} to reflect just the geometrical capacitance. We apply this same value for the semiconducting nanotube. The metallic nanotube under study has been assigned as a (18, 3) species based on simultaneous observations of Rayleigh and Raman RBM frequency (not shown). The difference in diameter between this nanotube and our near-zigzag semiconducting nanotube employed in the measurements shown in Fig. 2 is only expected to give rise to a difference in geometrical capacitance of $\sim$3% with an assumption of its logarithmic dependence on the nanotube diameter.

APPENDIX B: DETAILED THEORETICAL TREATMENT FOR THE ENERGY SHIFT

We have analyzed the influence of carrier density on the excitonic transition energies within the $\boldsymbol{k}\cdot\boldsymbol{p}$ scheme. The approach involves solving the Bethe-Salpeter (BS) equation [2,42],

$$E\psi_k = [(E_{c,k} + \Sigma_{c,k}) - (E_{v,k} + \Sigma_{v,k})]\psi_k - \sum_q K_{k,k+q}\psi_{k+q}. \tag{B1}$$

Here E is a complex quantity, corresponding to the exciton energy and the linewidth [72], k and q denote wave vectors, $E_{c(v),k}$ is the single-particle band energy, $\Sigma_{c(v),k}$ is the self-energy of the conduction (valence) band, and $K_{k,k+q}$ is the Coulomb interaction kernel. In the calculation, the exciton states are determined by a circumferential length $L_{\mathrm{c}}(=\pi d)$ of the nanotube, the characteristic kinetic energy $2\pi\gamma/L_{\mathrm{c}}$ [$\gamma = (\sqrt{3}/2)a\gamma_0$ with nearest-neighbor hopping integral $\gamma_0 = 2.7\,\mathrm{eV}$ and the lattice constant $a = 2.46$ Å of graphene], and the characteristic Coulomb energy $e^2/\kappa L_{\mathrm{c}}$, where κ is the effective dielectric constant from the effects of polarization of surrounding materials and electrons far from the Fermi level. The dimensionless Coulomb parameter $v = (e^2/\kappa)/(2\pi\gamma)$ represents the Coulomb interaction $e^2/\kappa L_{\mathrm{c}}$ scaled by the characteristic kinetic energy. In the calculations, we set $v = 0.16$, corresponding to $\kappa = 2.5$.

For calculation of the energy shift, we consider only intravalley scattering near the K (K') valley of the graphene Brillouin zone. We calculate a length-scale (q) dependent screened Coulomb interaction $W(q)$ within the static random-phase approximation [2,42]. The variation with carrier density is dominated by the q-dependent dielectric function $\varepsilon(q)$, which in turn depends on the Fermi energy through the Fermi distribution function. $\varepsilon(q)$ screens the Fourier component of the bare Coulomb interaction $V(q)$ as $W(q) = V(q)/\varepsilon(q)$. The self-energy $\Sigma_{c(v),k}$ is calculated within the screened Hartree-Fock approximation.

We evaluate the dielectric screening induced by the carrier doping within a static random-phase approximation. The dielectric function is expressed as [2,42]

$$\varepsilon_{n-m}(q) = 1 + \left[\Pi^K_{n-m}(q) + \Pi^{K'}_{n-m}(q)\right]V_{n-m}(q), \tag{B2}$$

where q is the wave vector of the external potential; n, m are the band indices that specify the 1D cutting lines of the nanotube in the graphene Brillouin zone; and $\Pi^{K(K')}_{n-m}(q)$ is the polarization function of the K (K') valley. $V_{n\text{-}m}(q)$ is calculated as

$$V_{n-m}(q) = \left(\frac{2e^2}{\kappa}\right) I_{|n-m|}(|q|d/2)K_{|n-m|}(|q|d/2), \tag{B3}$$

where I and K are modified Bessel functions. $\Pi^K_{n-m}(q)$ is calculated from the relation

$$\Pi^K_{n-m}(q) = -\frac{2}{A}\sum_{\alpha',\beta'}\sum_{k'} g_c\delta_{n-m,n'-m'}\left|M^K_{\beta'k',\alpha'k'+q}\right|^2 \times\left[\frac{f_{\alpha',k'+q}(1-f_{\beta',k'})}{E^K_{\alpha'}(k'+q) - E^K_{\beta'}(k') + i\delta} - \frac{(1-f_{\alpha',k'+q})f_{\beta',k'}}{E^K_{\alpha'}(k'+q) - E^K_{\beta'}(k') - i\delta}\right], \tag{B4}$$

where M is the scattering matrix element, A is the nanotube length, $E(k)$ is the energy of corresponding bands, g_{c} is the energy cutoff function, $f_{\alpha,k}$ is the Fermi distribution function for $E^K_\alpha(k)$, and the subscripts (α, β) specify the energy bands. A finite imaginary part $\delta/(2\pi\gamma/L_{\mathrm{c}}) = 0.1$ is introduced in the calculation. The effect of the free-carrier doping is taken into account through the change of the Fermi energy in the Fermi distribution function.

APPENDIX C: DETAILED THEORETICAL TREATMENT FOR THE LINEWIDTH BROADENING

Our theoretical treatment for the peak shift within the $\boldsymbol{k}\cdot\boldsymbol{p}$ scheme described above also predicts the exciton linewidth as the imaginary part of E in Eq. (B1). We found, however, that the calculated additional linewidth is nearly constant for finite carrier densities of $\rho > 0.05\ e/\mathrm{nm}$, and the linear increase of the linewidth observed in the experiment is not reproduced within this theory. This nearly constant linewidth can be understood as a consequence of a dominant contribution of intraband, low-energy scattering processes involving electrons near the Fermi surface to the calculated linewidth under sufficiently carrier-doped conditions, where the electronic density of states becomes nearly constant due to hyperbolic band structure of a semiconducting nanotube.

To address this discrepancy, we explored possible contributions to the linewidth arising from the *intervalley* (K-K') interactions that were omitted within treatment of the $\boldsymbol{k}\cdot\boldsymbol{p}$ approximation, as we now discuss. The scattering rate of a

photoexcited carrier from the doping in electron-doped nanotubes can be expressed within the second-order perturbation theory as

$$\Gamma_e^L = \frac{4\pi A_0^2}{(2\pi^2 d)^2} \sum_{l_1 l_2 (l_3 = L + l_1 - l_2)} \int dk \int dq |M_\nu|^2 \times \delta\left(e_0^L + e_k^{l_1} - e_q^{l_2} - e_{k-q}^{l_3}\right) f_k^{l_1} \left(1 - f_q^{l_2}\right)\left(1 - f_{k-q}^{l_3}\right),$$

$$\Gamma_h^L = \frac{4\pi A_0^2}{(2\pi^2 d)^2} \sum_{l_1 l_2 (l_3 = L + l_1 - l_2)} \int dk \int dq |M_\nu|^2 \times \delta\left(h_0^L + e_k^{l_1} - h_q^{l_2} - e_{k-q}^{l_3}\right) f_k^{l_1} f_q^{l_2} \left(1 - f_{k-q}^{l_3}\right), \quad \text{(C1)}$$

where index $\nu = (k, q, l_1, l_2, l_3)$, M_ν is the matrix element corresponding to the Coulomb coupling strength [60], $A_0 = a^2\sqrt{3}/2$, and twofold spin degeneracy of the carriers in the first subband has been included. Symbols e_k^l and h_k^l label the absolute energies of the carriers in the conduction and valence bands, respectively, with respect to the nanotube mid gap, and L, l are the angular momentum. The Fermi distribution functions f_k^l depend on the doping level and temperature, here $T = 300$ K. In this analysis of relaxation rates, we neglect the excitonic character of the optical excitations, assuming that the broadening can be modeled adequately in terms of the electron and hole dynamics of the underlying states comprising the exciton.

Within this approximation, Eq. (C1) implies an additional S_{33} and S_{44} linewidth given by the sum $\Gamma_e^L + \Gamma_h^L$. Because of the electron-hole symmetry in our theoretical treatment, the same scattering rate is obtained in a hole-doped nanotube, but applies equally well for electron-doped nanotubes. The calculated decay rates of the third and fourth excited states as a function of doping are shown in Fig. 4(b). The agreement with the data is surprisingly good considering that our calculations do not use any adjustable parameters [the value of $\kappa(= 2.5)$ is chosen to reproduce the energy shift]. This agreement may be partly fortuitous, due to the cancelation of the excitonic effects not included in evaluating matrix elements by the change of the dielectric response with doping.

The photoexcited electron of the S_{33} state has angular momentum $|L| = 4$, and e_0^4 in the K valley decays primarily into a finite q-momentum state in the second subband in K' valley $(l_2 = 2)\, e_q^2$ by promoting a first conduction band electron $(l_1 = -1)\, e_k^{-1}$ in the K' valley into the state $(l_3 = 1)\, e_{k-q}^1$ in the K valley with the opposite angular momentum. (Here we use the notation e_q^l for an electron with angular momentum l and momentum q). This scattering process is shown schematically in Fig. 6 and can be summarized as $e_0^4 + e_k^{-1} \rightarrow e_q^2 + e_{k-q}^1$. The excited photohole h_0^4 has two decay channels: $e_k^1 + h_q^1 \rightarrow h_0^4 + e_{k-q}^{-2}$ and $e_k^1 + h_q^2 \rightarrow h_0^4 + e_{k-q}^{-1}$, both giving about 66% of the total width of S_{33}. The first process, $e_k^1 + h_q^1 \rightarrow h_0^4 + e_{k-q}^{-2}$, in the (26, 0) nanotube, contributes only 25% to Γ_h^4.

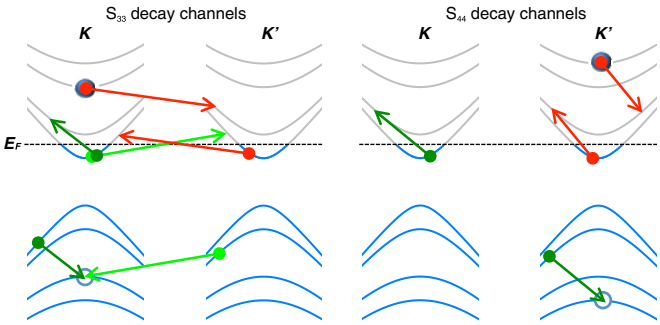

FIG. 6. (Color online) Schematic representation of the electronic band structure of a nanotube near the K and K' valleys and possible electron (hole) scattering pathways (pairs of arrows with the same colors) contributing to the observed increase in linewidth. Only the case for an electron-doped nanotube is shown. For S_{33} (S_{44}), only the pathways where a photoexcited electron and a hole in K (K') valley are involved are shown.

The photoexcited electron of the S_{44} state has angular momentum $|L| = 5$, and electron e_0^5 in the K' valley decays primarily into a finite q-momentum state in the second subband $(l_2 = 2)\, e_q^2$ by promoting a first conduction band electron $(l_1 = -1)\, e_k^{-1}$ in the K' valley into the state $(l_3 = 2)\, e_{k-q}^2$ in the K' valley with the opposite angular momentum. This process is shown schematically in Fig. 6 and can be described as $e_0^5 + e_k^{-1} \rightarrow e_q^2 + e_{k-q}^2$. The photoexcited hole h_0^5 has only one decay channel: $e_k^1 + h_q^2 \rightarrow h_0^5 + e_{k-q}^{-2}$ giving about 40% of the total width of S_{44}, which explains the slightly smaller doping-induced width observed experimentally for the S_{44} exciton compared to that of the S_{33} exciton.

As expected, a peak shift also arises from these intervalley scattering processes. The calculated shift for S_{33} at $\rho = 0.42\, e/\text{nm}$ (~2.6 meV) is, however, far smaller than the experimental shift (~60 meV) in Fig. 3. Hence, we can safely neglect the effect of the intervalley processes in describing doping-induced shifts of the excitonic transition energies.

[1] T. Ogawa and T. Takagahara, Phys. Rev. B **44**, 8138 (1991).
[2] T. Ando, J. Phys. Soc. Jpn. **66**, 1066 (1997).
[3] F. Wang, G. Dukovic, L. E. Brus, and T. F. Heinz, Science **308**, 838 (2005).
[4] J. Maultzsch, R. Pomraenke, S. Reich, E. Chang, D. Prezzi, A. Ruini, E. Molinari, M. S. Strano, C. Thomsen, and C. Lienau, Phys. Rev. B **72**, 241402(R) (2005).
[5] Y.-Z. Ma, L. Valkunas, S. M. Bachilo, and G. R. Fleming, J. Phys. Chem. B **109**, 15671 (2005).
[6] C. L. Kane and E. J. Mele, Phys. Rev. Lett. **93**, 197402 (2004).
[7] C. D. Spataru, S. Ismail-Beigi, L. X. Benedict, and S. G. Louie, Phys. Rev. Lett. **92**, 077402 (2004).
[8] V. Perebeinos, J. Tersoff, and P. Avouris, Phys. Rev. Lett. **92**, 257402 (2004).
[9] H. Zhao and S. Mazumdar, Phys. Rev. Lett. **93**, 157402 (2004).
[10] M. Bockrath, D. H. Cobden, P. L. McEuen, N. G. Chopra, A. Zettl, A. Thess, and R. E. Smalley, Science **275**, 1922 (1997).
[11] L. Marty, E. Adam, L. Albert, R. Doyon, D. Ménard, and R. Martel, Phys. Rev. Lett. **96**, 136803 (2006).

[12] P. Avouris, M. Freitag, and V. Perebeinos, Nat. Photonics **2**, 341 (2008).
[13] M. Steiner, M. Freitag, V. Perebeinos, A. Naumov, J. P. Small, A. A. Bol, and P. Avouris, Nano Lett. **9**, 3477 (2009).
[14] A. W. Bushmaker, V. V. Deshpande, S. Hsieh, M. W. Bockrath, and S. B. Cronin, Phys. Rev. Lett. **103**, 067401 (2009).
[15] M. J. O'Connell, S. M. Bachilo, C. B. Huffman, V. C. Moore, M. S. Strano, E. H. Haroz, K. L. Rialon, P. J. Boul, W. H. Noon, C. Kittrell, J. Ma, R. H. Hauge, R. B. Weisman, and R. E. Smalley, Science **297**, 593 (2002).
[16] S. M. Bachilo, M. S. Strano, C. Kittrell, R. H. Hauge, R. E. Smalley, and R. B. Weisman, Science **298**, 2361 (2002).
[17] T. Hertel, R. Fasel, and G. Moos, Appl. Phys. A **75**, 449 (2002).
[18] G. N. Ostojic, S. Zaric, J. Kono, M. S. Strano, V. C. Moore, R. H. Hauge, and R. E. Smalley, Phys. Rev. Lett. **92**, 117402 (2004).
[19] J. Kono, G. N. Ostojic, S. Zaric, M. S. Strano, V. C. Moore, J. Shaver, R. H. Hauge, and R. E. Smalley, Appl. Phys. A **78**, 1093 (2004).
[20] A. Jorio, C. Fantini, M. A. Pimenta, R. B. Capaz, G. G. Samsonidze, G. Dresselhaus, M. S. Dresselhaus, J. Jiang, N. Kobayashi, A. Grüneis, and R. Saito, Phys. Rev. B **71**, 075401 (2005).
[21] G. N. Ostojic, S. Zaric, J. Kono, V. C. Moore, R. H. Hauge, and R. E. Smalley, Phys. Rev. Lett. **94**, 097401 (2005).
[22] M. Y. Sfeir, T. Beetz, F. Wang, L. Huang, X. M. H. Huang, M. Huang, J. Hone, S. O'Brien, J. A. Misewich, T. F. Heinz, L. Wu, Y. Zhu, and L. E. Brus, Science **312**, 554 (2006).
[23] F. Wang, M. Y. Sfeir, L. Huang, X. M. Henry Huang, Y. Wu, J. Kim, J. Hone, S. O'Brien, L. E. Brus, and T. F. Heinz, Phys. Rev. Lett. **96**, 167401 (2006).
[24] L. Cognet, D. A. Tsyboulski, J.-D. R. Rocha, C. D. Doyle, J. M. Tour, and R. B. Weisman, Science **316**, 1465 (2007).
[25] A. G. Walsh, A. N. Vamivakas, Y. Yin, S. B. Cronin, M. S. Ünlü, B. B. Goldberg, and A. K. Swan, Nano Lett. **7**, 1485 (2007).
[26] K. Sato, R. Saito, J. Jiang, G. Dresselhaus, and M. S. Dresselhaus, Phys. Rev. B **76**, 195446 (2007).
[27] A. Das, A. K. Sood, A. Govindaraj, A. M. Saitta, M. Lazzeri, F. Mauri, and C. N. R. Rao, Phys. Rev. Lett. **99**, 136803 (2007).
[28] Y. Wu, J. Maultzsch, E. Knoesel, B. Chandra, M. Huang, M. Y. Sfeir, L. E. Brus, J. Hone, and T. F. Heinz, Phys. Rev. Lett. **99**, 027402 (2007).
[29] J. Lefebvre and P. Finnie, Nano Lett. **8**, 1890 (2008).
[30] L. Lüer, S. Hoseinkhani, D. Polli, J. Crochet, T. Hertel, and G. Lanzani, Nat. Phys. **5**, 54 (2008).
[31] S. Berciaud, C. Voisin, H. Yan, B. Chandra, R. Caldwell, Y. Shan, L. E. Brus, J. Hone, and T. F. Heinz, Phys. Rev. B **81**, 041414(R) (2010).
[32] J. Deslippe, M. Dipoppa, D. Prendergast, M. V. O. Moutinho, R. B. Capaz, and S. G. Louie, Nano Lett. **9**, 1330 (2009).
[33] I. V. Bondarev, L. M. Woods, and K. Tatur, Phys. Rev. B **80**, 085407 (2009).
[34] Y. Murakami and J. Kono, Phys. Rev. Lett. **102**, 037401 (2009).
[35] Y. Miyauchi, H. Hirori, K. Matsuda, and Y. Kanemitsu, Phys. Rev. B **80**, 081410(R) (2009).
[36] C. D. Spataru and F. Léonard, Phys. Rev. Lett. **104**, 177402 (2010).
[37] S. Yasukochi, T. Murai, S. Moritsubo, T. Shimada, S. Chiashi, S. Maruyama, and Y. K. Kato, Phys. Rev. B **84**, 121409(R) (2011).
[38] R. Matsunaga, K. Matsuda, and Y. Kanemitsu, Phys. Rev. Lett. **106**, 037404 (2011).
[39] S. M. Santos, B. Yuma, S. Berciaud, J. Shaver, M. Gallart, P. Gilliot, L. Cognet, and B. Lounis, Phys. Rev. Lett. **107**, 187401 (2011).
[40] J. R. Schneck, A. G. Walsh, A. A. Green, M. C. Hersam, L. D. Ziegler, and A. K. Swan, J. Phys. Chem. A **115**, 3917 (2011).
[41] H. Farhat, S. Berciaud, M. Kalbac, R. Saito, T. F. Heinz, M. S. Dresselhaus, and J. Kong, Phys. Rev. Lett. **107**, 157401 (2011).
[42] Y. Tomio, H. Suzuura, and T. Ando, Phys. Rev. B **85**, 085411 (2012).
[43] K. Liu, J. Deslippe, F. Xiao, R. B. Capaz, X. Hong, S. Aloni, A. Zettl, W. Wang, X. Bai, S. G. Louie, E. Wang, and F. Wang, Nat. Nanotechnol. **7**, 325 (2012).
[44] S. Mouri and K. Matsuda, J. Appl. Phys. **111**, 094309 (2012).
[45] S. Konabe, K. Matsuda, and S. Okada, Phys. Rev. Lett. **109**, 187403 (2012).
[46] L. Colombier, J. Selles, E. Rousseau, J. S. Lauret, F. Vialla, C. Voisin, and G. Cassabois, Phys. Rev. Lett. **109**, 197402 (2012).
[47] J. S. Park, Y. Hirana, S. Mouri, Y. Miyauchi, N. Nakashima, and K. Matsuda, J. Am. Chem. Soc. **134**, 14461 (2012).
[48] T. Nishihara, Y. Yamada, and Y. Kanemitsu, Phys. Rev. B **86**, 075449 (2012).
[49] Y. Kimoto, M. Okano, and Y. Kanemitsu, Phys. Rev. B **87**, 195416 (2013).
[50] B. Yuma, S. Berciaud, J. Besbas, J. Shaver, S. Santos, S. Ghosh, R. B. Weisman, L. Cognet, M. Gallart, M. Ziegler, B. Hönerlage, B. Lounis, and P. Gilliot, Phys. Rev. B **87**, 205412 (2013).
[51] T. Koyama, S. Shimizu, Y. Miyata, H. Shinohara, and A. Nakamura, Phys. Rev. B **87**, 165430 (2013).
[52] K. Liu, X. Hong, Q. Zhou, C. Jin, J. Li, W. Zhou, J. Liu, E. Wang, A. Zettl, and F. Wang, Nat. Nanotechnol. **8**, 917 (2013).
[53] S. Schäfer, N. M. B. Cogan, and T. D. Krauss, Nano Lett. **14**, 3138 (2014).
[54] Y. Kumamoto, M. Yoshida, A. Ishii, A. Yokoyama, T. Shimada, and Y. K. Kato, Phys. Rev. Lett. **112**, 117401 (2014).
[55] D. Stich, F. Spath, H. Kraus, A. Sperlich, V. Dyakonov, and T. Hertel, Nat. Photonics **8**, 139 (2013).
[56] T. Mori, Y. Yamauchi, S. Honda, and H. Maki, Nano Lett. **14**, 3277 (2014).
[57] N. Akizuki, M. Iwamura, S. Mouri, Y. Miyauchi, T. Kawasaki, H. Watanabe, T. Suemoto, K. Watanabe, K. Asano, and K. Matsuda, Phys. Rev. B **89**, 195432 (2014).
[58] E. H. Hároz, J. G. Duque, E. B. Barros, H. Telg, J. R. Simpson, A. R. Hight Walker, C. Y. Khripin, J. A. Fagan, X. Tu, M. Zheng, J. Kono, and S. K. Doorn, Phys. Rev. B **91**, 205446 (2015).
[59] M. Jiang, Y. Kumamoto, A. Ishii, M. Yoshida, T. Shimada, and Y. K. Kato, Nat. Commun. **6**, 6335 (2015).
[60] V. Perebeinos and P. Avouris, Phys. Rev. B **74**, 121410(R) (2006).
[61] T. Takenobu, T. Takano, M. Shiraishi, Y. Murakami, M. Ata, H. Kataura, Y. Achiba, and Y. Iwasa, Nat. Mater. **2**, 683 (2003).
[62] M. S. Strano, C. B. Huffman, V. C. Moore, M. J. O'Connell, E. H. Haroz, J. Hubbard, M. Miller, K. Rialon, C. Kittrell, S. Ramesh, R. H. Hauge, and R. E. Smalley, J. Phys. Chem. B **107**, 6979 (2003).
[63] L. Huang, X. Cui, B. White, and S. P. O'Brien, J. Phys. Chem. B **108**, 16451 (2004).
[64] S. Berciaud, V. V. Deshpande, R. Caldwell, Y. Miyauchi, C. Voisin, P. Kim, J. Hone, and T. F. Heinz, Phys. Status Solidi B **249**, 2436 (2012).

[65] See Supplemental Material at http://link.aps.org/supplemental/10.1103/PhysRevB.92.205407 for the Rayleigh scattering results for positive gating voltages and evaluation of the effect of strain.
[66] M. Huang, Y. Wu, B. Chandra, H. Yan, Y. Shan, T. F. Heinz, and J. Hone, Phys. Rev. Lett. **100**, 136803 (2008).
[67] J. O'Keeffe, C. Wei, and K. Cho, Appl. Phys. Lett. **80**, 676 (2002).
[68] A. V. Naumov, S. M. Bachilo, D. A. Tsyboulski, and R. B. Weisman, Nano Lett. **8**, 1527 (2008).
[69] T. Takenobu, Y. Murayama, and Y. Iwasa, Appl. Phys. Lett. **89**, 263510 (2006).
[70] J. C. Tsang, M. Freitag, V. Perebeinos, J. Liu, and P. Avouris, Nat. Nanotechnol. **2**, 725 (2007).
[71] S. Ilani, L. A. K. Donev, M. Kindermann, and P. L. McEuen, Nat. Phys. **2**, 687 (2006).
[72] G. Strinati, Phys. Rev. B **29**, 5718 (1984).